https://doi.org/10.5194/egusphere-2024-2138
Preprint. Discussion started: 8 January 2025

Experimental study on granite weathered crust landslides with different residual layer thicknesses under heavy rainfall

Jingye Chen[1,2], Qinghua Gong[2], Jun Wang[2], and Shaoxiong Yuan[2]

[1]College of Civil Engineering&Architecture, China Three Gorges University, Yichang 443002, China
[2]Guangzhou Institute of Geography, Guangdong Academy of Science, Guangzhou 510070, China

Correspondence: Qinghua Gong (gqh100608@163.com)

Abstract. Granite weathered crust exhibits a dual structure, which affects the pattern of damage on slopes. This study designed three kinds of slope models with residual layer thicknesses against the background of a landslide cluster in Mibei Village, Longchuan County, Guangdong Province. The hydrological response and deformation damage characteristics of granite weathered crust slopes under heavy rainfall conditions were analyzed and the disaster-causing mechanism of landslides was studied through physical model tests. The results show that the three types of slopes exhibit distinct disaster mechanisms. For the slope with a residual layer of 10 cm thickness, rainfall rapidly infiltrates the soil-rock interface, resulting in the formation of a temporary water table at the interface. The residual layer is rapidly saturated and is susceptible to overall flow-slip damage under seepage, with no obvious sliding surface. For the slope with a residual layer of 20 cm thickness, it takes a long time for rainfall to penetrate into the soil-rock interface. Rainwater gathered at the interface significantly reduces the shear strength of the residual soil. Slope tends to slide along the soil-rock interface at the slope toe under the traction and drag of water flow, which can result in sudden slide. For the slope with a residual layer of 10cm thickness, no evidence of strong seepage is observed within the slope. The slope gradually slides along the wetting front under hydrostatic pressure and self-sliding force, with the circular arc sliding surface.

1 Introduction

Granite is widely distributed in the southeastern coastal areas of China. The area of granite in Guangdong Province is approximately 65,300 km², which accounts for about 36% of the total area of the province (Zhang 2009). The granite is subjected to a lengthy period of physico-chemical weathering to form a huge thick weathered crust with a surface layer of granite residual soil. The residual soil exhibits superior integrity and remarkable mechanical properties due to the robust interconnections between weathering residues (Chen et al. 2011). However, residual soil exhibits poor hydro-physical characteristics, rendering its original stable structure susceptible to rapid destruction when exposed to water (Branco et al. 2014; An et al. 2020; Li et al. 2020). Wang et al. (2020) demonstrated that slope stability is reduced by up to 30% under wet and dry cycles. Guangdong Province is situated within the subtropical monsoon climate zone, characterized by abundant rainfall. The granite area is prone to group-occurring mountain disasters during heavy rain. For example, Typhoon *Fanyabi* precipitated exceptionally heavy precipitation in Magui Town on September 21, 2010, resulting in a geologic catastrophe that claimed 100 lives, affected 129,000 individuals, and incurred 5.15 billion RMB in direct economic losses (Wang et al. 2022). From June 9 to 14, 2019, Longchuan County experienced persistent heavy precipitation, resulting in numerous landslides and debris flows throughout the county. The event affected 24 towns and 352 villages to varying degrees (Bai et al. 2021). These disasters have caused considerable economic and ecological losses within the region.

Rainfall infiltration results in the softening and increased weight of the rock and soil. From a hydrologic perspective, it causes runoff within the slope and an increase in the water table. These factors are critical in inducing landslides (Iverson 2000; Zeng et al. 2017; Tang et al. 2018; Marin and Velai 2020). Scholars have conducted relevant research on landslides in granite areas by analyzing the hydrological response, mechanical relationship and structural change of slopes during rainfall. Wakatsuki and Matsukura (2008) concluded that granite slopes with thin weathered layers are more sensitive to rainfall response and more prone to landslides. Xia et al. (2019) demonstrated that the physico-mechanical properties of residual soil exhibit spatial variability along the profile, which has a significant impact for slope erosion. Herrada et al. (2014) and Xu et al. (2018) investigated the seepage field characteristics and evolution patterns of residual soil slopes under rainfall, establishing applicable seepage models. Harianto et al. (2010) concluded that changes in residual soil water content lead to corresponding changes in matrix suction, and the magnitude of matrix suction affects soil shear strength and slope stability. Zhang et al. (2020) analyzed the seepage and stress-strain fields of slopes by back-analyzing the unsaturated hydraulic parameters of residual soils using soil column tests and applying them to numerical simulations. Xu et al. (2018) and Bai et al. (2022) applied physical model tests to analyze the destabilization and damage process of slopes under different conditions to reveal the destabilization pattern of rainfall-induced residual soil slopes. Roberto et al. (2019) found that the damage process of residual soil slopes during precipitation is a complex process involving multiple initiations and destabilization. Feng et al. (2022) carried out an in-situ rainfall test in the granite area. The study initially revealed the damage mechanism of landslides by observing and analyzing the changes in

https://doi.org/10.5194/egusphere-2024-2138
Preprint. Discussion started: 8 January 2025

sensor data and the phenomenon of deformation and destruction.

The majority of current studies simplify the granite weathered crust as a single homogeneous soil layer. Nevertheless, there are notable discrepancies in the physico-mechanical properties of the residual and weathered layers of real-world granite weathered crust (Qi et al., 2022). Furthermore, the weathering degree of granite is influenced by geomorphological and climatic conditions, which often results in residual layers with significant thickness differences (Wang et al. 1991). The influence of stratigraphic structure must be considered if the diversity and complexity of slope damage in granite areas under heavy rainfall are to be fully explained. In this study, a detailed survey was conducted to inform the design of slope models, which were then subjected to physical model tests. The results analyze the hydrological response and the deformation and damage mechanisms of slopes with different residual layer thicknesses under heavy rainfall. This study can provide theoretical basis for the monitoring and prevention of rainfall-induced landslides in granite areas.

2 Background

Longchuan County, Guangdong Province, is located in the subtropical monsoon climate zone of China. The area experiences a high level of precipitation, with an average annual rainfall of 1621.79 mm. The distribution of rainfall across the region is uneven, with the majority of precipitation occurring between April and July each year. These months account for 52% of the annual rainfall, with the majority of this occurring as heavy rainfall. A total of 95.35% of geohazards occurred during periods of concentrated rainfall (Zhu 2021; Jia et al., 2024). There is a strong correlation between periods of heavy rainfall and periods of high incidence of geohazards. From June 10 to 13, 2019, persistent rainfall occurred in Longchuan County. One of the heavy rainfalls from 14:00 to 19:00 on June 11 resulted in mass landslides throughout the Mibei Village. Following the disaster, we surveyed the geological and geographic environment of Mibei Village, focusing on the 31 larger landslide sites in this event (Fig. 1b). The study area is hilly and mountainous landform, with simple geological conditions. There are no discernible faults or folds, and the groundwater table is deep. The bedrock consists of Lower Paleozoic granite. The outcrops on the surface expose the thick weathered crust formed by the weathering of granite. A distinct boundary can be seen in the profile of the stratum (Fig. 2a), showing a typical dual structure. The upper part of the weathered crust is the residual layer formed in situ after the weathering of granite. It is unevenly exposed at different locations and has a thickness of 1.00-10.40 m. The residual soil is hard plastic, slightly wet, and yellowish-brown in color. Quartz grains are visible to the naked eye. The lower part consists of the completely weathered layer, where the original rock structure remains discernible. The lower part of the weathered crust is the completely weathered layer, where the original rock structure remains recognizable. The completely weathered granite is hard and grayish-brown in color. All minerals, except for quartz, have been weathered (Fig. 2b). The basic geotechnical properties of the weathered crust are shown in Table 1. According to particle gradation, the residual soil belongs to sandy clay (Zhang et al. 1997). The lower completely weathered layer is more compact and less susceptible to water seepage than the upper residual layer. The survey statistics of 31 landslide points show that the slope gradient of the landslides ranges from 31° to 45°, with the transverse width from 36 to 135 m, and the longitudinal length from 40 to 88 m. The sliding surface depth ranges from 1.5 to 4.3 m, all of which are shallow landslides. The material composition of the landslide mass is mainly residual soil. The water content of the landslide mass is considerable, and some of the landslides exhibit fluidization.

https://doi.org/10.5194/egusphere-2024-2138
Preprint. Discussion started: 8 January 2025

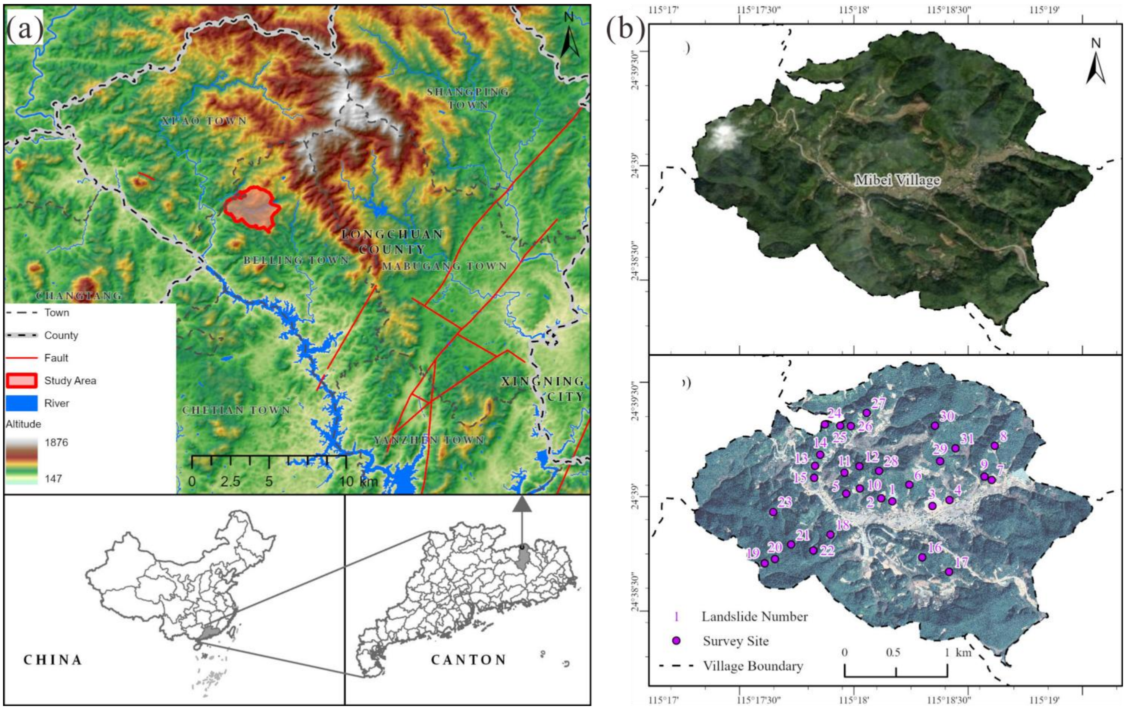

Figure 1. Map showing the background of study area. **(a)** geographical location. **(b)** satellite images before and after disaster (sourced from © Google Earth).

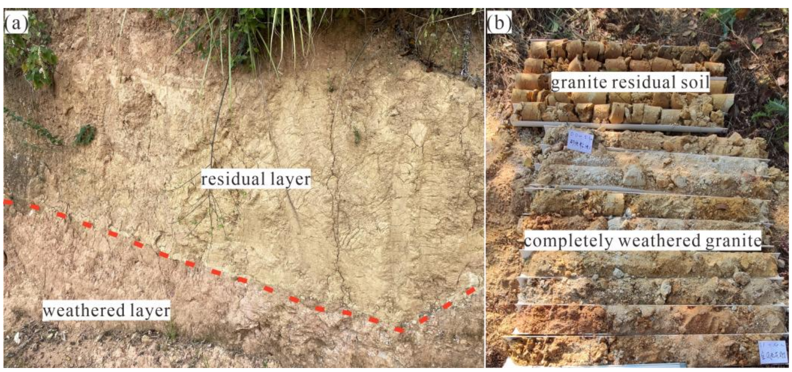

Figure 2. Geological condition of the study area. **(a)** stratigraphic structure. **(b)** core.

Table 1. Geotechnical properties of granite weathered crust.

Rock and soil	Dry density ($g \cdot cm^{-3}$)	Mass water content (%)	Void ratio	Permeability coefficient ($m \cdot s^{-1}$)	Soil mass percentage by grain size (%)				
					>2 mm	≤2 mm	≤0.5 mm	≤0.25 mm	≤0.075 mm
Residual soil	18.9	7.53	0.724	3.47×10^{-5}	6.49	93.51	56.39	46.91	39.63
Completely weathered granite	20.7	6.14	0.563	4.86×10^{-6}	10.79	89.21	57.44	44.81	31.41

3 Physical model test

3.1 Artificial rainfall model experiment

The slope physical model test platform is comprised of model box, rainfall system, and data acquisition system

https://doi.org/10.5194/egusphere-2024-2138
Preprint. Discussion started: 8 January 2025

(Fig. 3a). The dimension of the model box is 2 m×1 m×1.8 m (Length×Width×Height), and it is constructed with plexiglass and steel columns. Grid lines have been drawn on the plexiglass sidewalls to provide coordinate reference and datum control. The EL-RS3/5 mobile artificial rainfall simulation system produced by Beijing ECO-LEADER company that consists of rainfall machine, water supply system, control system. Its effective rainfall area is 5 m×3 m (Length× Width), with the rainfall uniformity coefficient greater than 0.9. The data acquisition system mainly consists of water content sensor, pore water pressure sensor, and data collector, which are produced by Xi'an Weizheng Electronic Technology Company. The water content and pore water pressure data are transferred to the notebook at a frequency of 3 min via the data collector. The deformation damage characteristics of slopes are recorded using the camera.

The objective of this experiment is to explore the rainfall infiltration law and the process of deformation damage in granite weathered crust slopes with varying residual layer thicknesses during heavy rainfall. A slope model geometric similarity ratio of 1:20 was determined based on the field investigation and experiment conditions. The model measures 120 cm in length, 100 cm in width, and has a slope angle of 27°. Three sets of test models, designated E1, E2 and E3, were designed with residual layer thicknesses of 10 cm, 20 cm and 30 cm, respectively. The generalized geological model is shown in Fig. 4. According to Weber similarity criterion, the rainfall intensity similarity ratio should be the negative one-half power of the geometric similarity ratio (Sun and Zhang 2012). Accordingly, this study employs the rainfall intensity similarity ratio of 1:0.22. The cumulative rainfall in the study area prior to the disaster was 62.4 mm from 14:00 to 19:00, which was converted to rainfall intensity 47.2 mm/h and duration 6h for the experiment. The groundwater table in the study area is deep, and the initiation of landslides is not related to groundwater. Therefore, groundwater is not considered in the test.

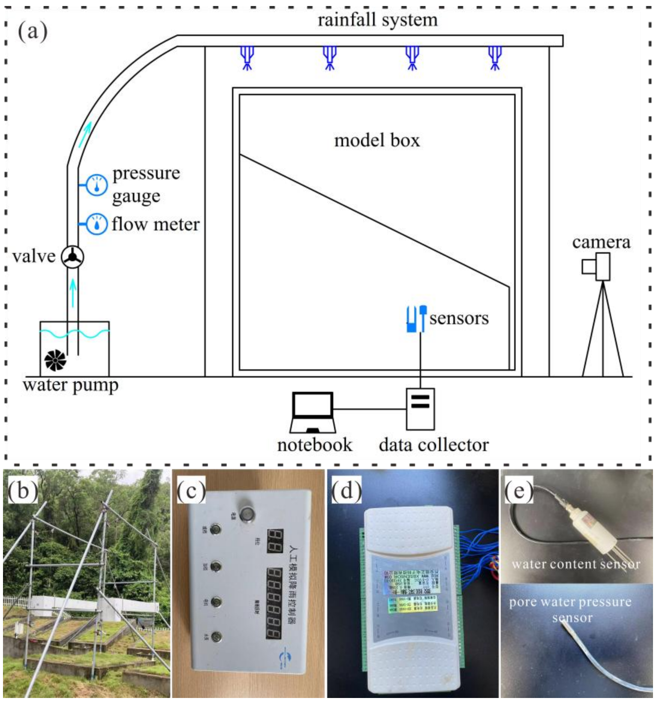

Figure 3. Slope physical model test platform. **(a)** model test system. **(b)** rainfall simulator. **(c)** rainfall controller. **(d)** data collector. **(e)** sensors.

https://doi.org/10.5194/egusphere-2024-2138
Preprint. Discussion started: 8 January 2025

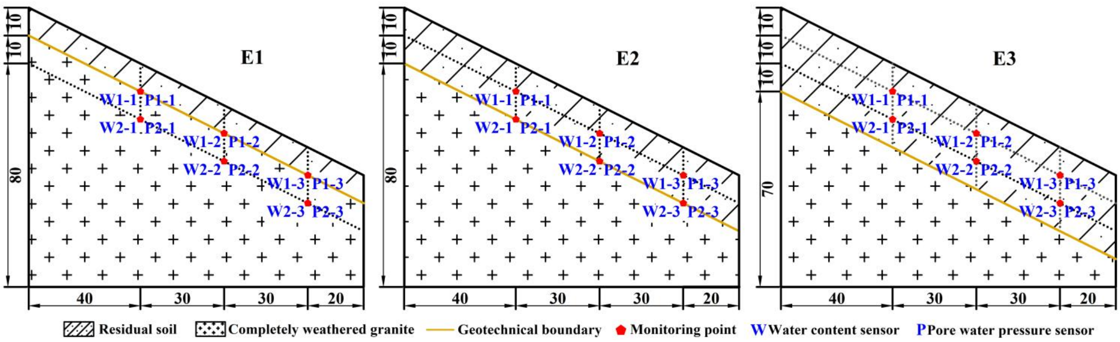

Figure 4. Schematic diagram of slope dimension and sensor buried position (unit: cm).

3.2 Material selection

The selection of experimental materials is the focus of physical model test. At present, two principal approaches to material selection exist. The first is the use of artificial materials configured based on similarity theory (Zhang et al. 2023; Li et al. 2023). The second is the use of prototypical materials taken directly from the study area (Zhang et al. 2019; Zhen et al. 2023). This experiment focuses on the impact of performance differences among geotechnical bodies on slope damage, so the selection of prototypical materials can more objectively reflect the rainfall infiltration law and deformation damage process of this type of slope. The experiment model comprises the residual layer and the weathered layer. Residual soil and completely weathered granite were first sampled in the landslide area and then remodeled indoors based on particle gradation and initial mass moisture content.

3.3 Experiment procedure

The slopes were modeled by combing the density control method and the layered filling method. The specific experimental procedure is as follows:

1. The slopes were filled in one layer per 10 cm. The mass of material needed to lay each layer was calculated using the volume of each modeled layer, the predetermined dry density and water content of the geotechnical body.
2. The weathered layer was filled first. The weighed material was spread evenly inside the model box and tamped to the predetermined height. The model was subsequently cut to the predetermined angle based on the gridlines of the sidewalls of the model box. To simulate the interface between the weathered and residual layer, the surface of the weathered layer was scraped. Repeated the aforementioned steps to complete the filling of the residual layer.
3. When the material was stacked to the depth of the sensor pre-embedding during slope construction, the sensor was inserted and secured while the data collector was turned on to determine if the readings are abnormal.
4. After completing the modeling, the model was covered with tarpaulin and left to stand for 48 h. This allowed for uniform adjustment of the internal water distribution and stress state of the soil body. Initiate the rainfall system to commence the experiment. The experiment was terminated if landslides occurred during rainfall.

4 Results

4.1 Slope failure process

Figure 5 shows the failure process of the E1 slope. The infiltration of rainwater into the slope resulted in the destruction of the soil structure, leading to the formation of small range of low lying areas on the slope (Fig. 5a). As rainfall persisted, the residual layer gradually became saturated, and runoff was generated on the slope. The low lying areas on the slope surface gradually developed into fine gullies as a result of runoff scouring (Fig. 5b). The phenomenon of slip-collapse was first observed at the slope toe (Fig. 5c). The initial fine gullies, subjected to the continuous action of seepage and erosion, ultimately evolved into erosion trenches of a certain depth and width (Fig. 5d). From the shape of the landslide, the E1 slope was severely eroded by the water flow, and there was no obvious sliding surface , showing an overall flow-slip damage (Fig. 5d). In terms of the landslide failure process, the extensive damage to the E1 slope occurred subsequent to the damage to the slope toe.

Figure 6 shows the failure process of the E2 slope. Rainwater was constantly flowing towards the slope toe, thereby reducing its capacity to withstand deformation damage and facilitating the formation of crack I in rainfall 294 min (Fig. 6a). At 306 min of rainfall, the soil body at the slope toe exhibited horizontal movement along the soil-rock

https://doi.org/10.5194/egusphere-2024-2138
Preprint. Discussion started: 8 January 2025

interface, resulting in uneven settlement of approximately 3 cm of downward misalignment and crack II (Fig. 6b). The slope then slid along crack I and crack II (Fig. 6c). From the shape of the landslide, the E2 landslide was characterized by a straight trailing edge and a translational sliding surface at the soil-rock interface (Fig. 6d). In terms of the slope failure process, It took only 15 min for the E2 slope to occur landslide after the appearance of the crack at the slope toe. This landslide was characterized by sudden sliding.

Figure 7 shows the failure process of the E3 slope. Rainfall infiltration alters the stress state within the slope, resulting in tensile stress concentration at the top and middle of the slope. Tensile crack I were observed under the influence of gravity (Fig. 7a). With the continuous heavy rainfall, the microcrack I further expanded. Concurrently, crack II appeared on the slope (Fig. 7b). The cracks continued to expand and penetrate. Eventually the landslide sheared out at the slope toe (Fig. 7c). From the shape of the landslide, The thickness of the E3 landslide was about 23 cm. The sliding surface exhibited a circular arc shape, which is rotational landslide (Fig. 7d). In terms of the slope failure process, the E3 slope tended to experience sliding due to the slow expansion and penetration of the crack situated at the middle of the slope. This process caused multiple cracks to appear on the slope, which was a progressive damage.

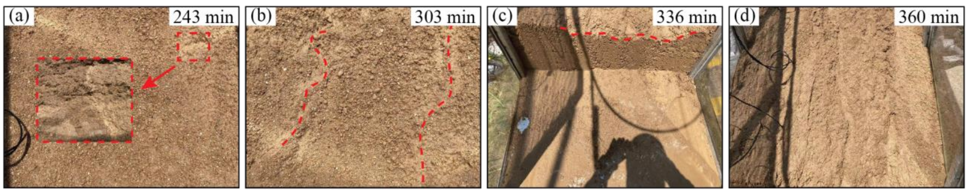

Figure 5. Deformation and failure process of E1 slope. **(a)** low lying area. **(b)** runoff scouring. **(c)** slip and collapse at slope toe. **(d)** surface erosion.

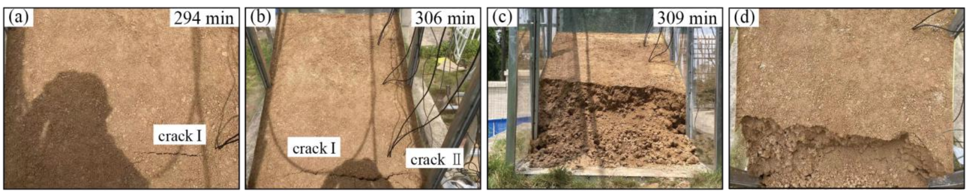

Figure 6. Deformation and failure process of E2 slope. **(a)** crack at slope toe. **(b)** slope dislocation. **(c)** landslide occurrence. **(d)** top view.

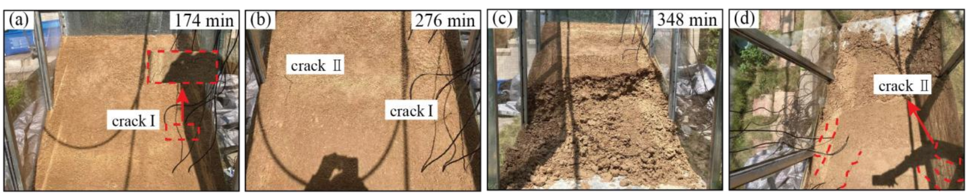

Figure 7. Deformation and failure process of E3 slope. **(a)** crack at mid-slope. **(b)** crack propagation. **(c)** landslide occurrence. **(d)** top view

4.2 Water content response

The water content-time curve for the E1 slope is presented in Fig. 8a. In the early stage of rainfall, rainwater infiltrated into the slope through the pores of the residual soil. After 57 min of rainfall, the values of W1-1 and W1-3 increased first, followed by W1-2, indicating that the rainfall had infiltrated to the interface between the residual layer and the weathered layer and that the water content of the soil near the soil-rock interface began to increase. Subsequently, the growth rate of W1-1, W1-2, and W1-3 values continued to increase. The values increased sharply and peaked within 135-159 min. This indicates that the soil water content at the soil-rock interface rises rapidly and the soil becomes saturated in a short period of time. The sensors within the weathered layer did not begin to respond until 267 min after rainfall, and the rate of increase in W2-1, W2-2, and W2-3 values was consistently low. At the conclusion of the test, it was observed that the largest increase in sensor value was only 3.38%. This suggests that rainfall has a minimal impact on the weathered layer. The phenomenon is attributed to the infiltration of rainwater into the weathered layer, which has a low permeability. The difference in permeability coefficients between the upper and lower geotechnical layers affects the rate

https://doi.org/10.5194/egusphere-2024-2138
Preprint. Discussion started: 8 January 2025

of rainwater infiltration at the interface, resulting in a notable reduction. The dense weathered layer in the lower part exhibits water resistance, and water stagnation occurs at the interface between the residual and weathered layers. Rainwater flows along the interface, reducing the vertical infiltration capacity and making it difficult to infiltrate into the weathered layer.

The water content-time curve for the E2 slope is presented in Fig. 8b. At the onset of rainfall, rainwater mainly infiltrated vertically into the shallow surface layer of the slope in the form of pore flow. The W1-1 value exhibited the earliest increase after 54 min of rainfall, due to the fact that the top of the slope is closest to the rainfall device and is more susceptible to rainfall infiltration. Subsequently, the values of W1-3 and W1-2 commenced an incremental ascent, signifying that the rainfall infiltration had reached a depth of 10 cm within the slope at that moment. After 111 min of rainfall, the W2-2 value began to increase, followed by W2-1 and W2-3. This indicates that the rainfall had infiltrated at the residual layer-weathered layer interface. The values of W2-1, W2-2 and W2-3 increased sharply, and their growth rate was much higher than that of the sensor at the soil burial depth of 10 cm. The cause of this phenomenon is analogous to that of E1 slope. The infiltration properties of the residual and weathered layer exert a significant influence on the accumulation of rainwater at the soil-rock interface, which subsequently forms a temporary water table. Rainwater that infiltrates into the soil-rock interface collects here affected by different infiltration properties of the residual and weathered layers. This results in the formation of a temporary water table. The water table gradually rises as rainfall infiltrates, and the water content of soil in the vicinity of the interface increases at a faster rate than that of soil above the interface. The values of W1-1, W1-2, and W1-3 remained stable after 153 min, 141 min, and 168 min, respectively. This indicates that the soil at a depth of 20 cm had reached saturation. At 273 min of rainfall, the W1-3 value showed a pronounced increase, suggesting that the rate of increase of soil water content at the depth of 10 cm at the slope toe was considerably more rapid. This is due to the fact that rainwater continues to collect at the slope toe under the influence of runoff, and the subsequent rise in the temporary water table to the depth of 10 cm. As the rainfall continued, the soil water content at the slope toe eventually became significantly higher than that at the top and middle of the slope, reaching saturation after 291 min of rainfall.

The water content-time curve for the E3 slope is presented in Fig. 8c. During the initial 60 min of rainfall, the infiltration of rainwater into the 10 cm depth of soil occurred in the form of pore flow, resulting in a sequential increase in the values of W1-1, W1-3, and W1-2. Following 138 min of rainfall, the W2-3 value began to increase, indicating that rainwater infiltrated to the depth of 20 cm at the slope toe. This was followed by a sequential increase in the values of W2-1 and W2-2. At 200 min of rainfall, the growth range of each sensor value was W1-3>W1-1>W1-2>W2-3>W2-1>W2-2. This shows that the rate of water content growth in the soil at the depth of 20 cm is significantly slower than that at the depth of 10 cm. It is because the transport of infiltrating rainwater to greater depths is affected by the unsaturated permeability of the soil at the wetting front, where the soil is still in the state of initial matrix suction. The low unsaturated permeability of the soil at the wetting front hinders the vertical downward movement of water (Rahardjo et al. 2005). The mode of rainfall transport has undergone a significant shift, moving from a predominantly vertical infiltration process to one that coexists with horizontal percolation. This shift has resulted in notable delay in the response of the deeper part of the slope to rainfall infiltration. In addition, rainwater within the infiltration slope continued to converge downward under gravity, resulting in the most rapid increase in sensor value at the slope toe. The W1-2 value showed a significant increasing trend following 258 min of rainfall, indicating a swift rise in soil water content at the depth of 10 cm within the slope. The reason for this phenomenon is that the crack at the middle of slope provide easy access for rainfall infiltration. Rainwater infiltrates rapidly in the form of crack-preferential flow. The peak values of W1-3, W1-1, and W1-2 were observed at 288, 303, and 321 min of rainfall, respectively, indicating that the soil was nearly saturated at the depth of 10 cm.

https://doi.org/10.5194/egusphere-2024-2138
Preprint. Discussion started: 8 January 2025

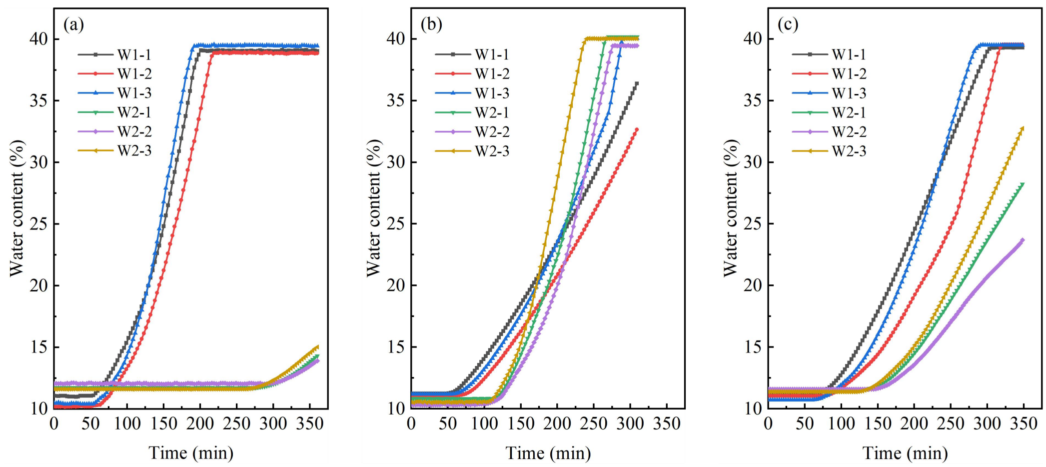

Figure 8. Water content-time curves. **(a)** E1 slope. **(b)** E2 slope. **(c)** E3 slope.

4.3 Fine particle migration

In the case of rainfall-induced landslides, it is common for turbid runoff to carry sediment downhill and pile up at the slope toe. The phenomenon is essentially particle migration (Lu et al. 2011; Cui et al. 2014). The residual soil lacks intermediate particle size. The coarse particles form the skeleton of the soil, and the fine particles are attached to the skeleton particles as cement-like substance (Liu et al. 2021). This makes the fine particles can be carried by water flow and move through the skeleton pore. It is difficult to make direct observation inside the slope without the aid of specialized equipment. In this study, Samples were obtained from the top, middle, and toe of slope of the three groups using cutting ring. The locations of the samples were correspond with the depth of the sliding surface. The fine particles (particle size less than 0.075 mm) in the soil were measured by the particle gradation test, which was then compared with the initial fine particle content.

The fine particle content at each location of the slopes at the end of the tests is shown in Fig. 9. It can be seen that there is a large difference in the fine particle content at each location of E1 slope. The loss of fine particles was most severe at the top of the slope, with a reduction from an initial 39.63% to 30.61%. The loss of fine particle content in the middle of slope was then 7.42%. Concurrently, the fine particle content at the toe of the slope increased by 8.53% (Fig. 9a). This indicates that the interior of the slope was undergoing a process of fine particle loss, with the lost portion undergoing longitudinal migration and eventual accumulation at the toe of the slope. The fine particle content of E2 slope exhibited a 3.18% decrease at the top of the slope, a 1.16% decrease at the middle of the slope, and a 2.51% increase at the slope toe (Fig. 9b). E2 slope have been observed to exhibit a substantial reduction in fine particle loss in comparison to E1 slope. This is due to the fact that the seepage time in the E2 slope was relatively brief, with seepage occurring only locally. The fine particle content is nearly identical at all locations in the E3 slope (Fig. 9c). This phenomenon may be attributed to the absence of pronounced seepage in the E3 slope, which had resulted in a low likelihood of fine particle migration. The loss of fine particles destroys the soil structure, which has a greater impact on slope stability. The gradual increase in pore size between coarse particles within the slope will in turn exacerbate the loss of fine particles, leading to a reduction in the strength of slopes and their susceptibility to damage.

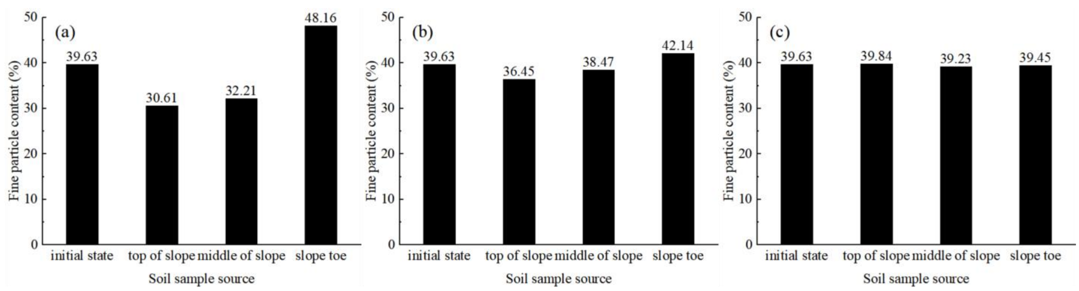

Figure 9. Fine particle content at different positions of slopes with different tests. **(a)** E1 slope. **(b)** E2 slope. **(c)** E3 slope.

4.4 Pore water pressure response

https://doi.org/10.5194/egusphere-2024-2138
Preprint. Discussion started: 8 January 2025

The water content change curve indicates that the initial state of the soil and rock mass of the slope model is unsaturated. The slope exhibits a significant matrix suction, which necessitates the use of a high-capacity tension sensor for measurement. However, the pore water pressure sensor utilized in this study is only capable of measuring positive pore water pressure. Therefore, the value of the sensor was set to zero prior to the commencement of the test (Nian et al., 2023).

The pore water pressure-time curves are presented in Fig. 10. In general, the pore water pressure change curves exhibit a similar overall trend to the water content change curves. This is due to the fact that the change in pore water pressure in the soil is primarily influenced by the soil water content. The value of P1-1 in the E1 test exhibited a slight decline at 261 min of rainfall, followed by a rapid increase at 273 min of rainfall (Fig. 10a). This phenomenon may be attributed to the loss of fine particles from the soil, which results in the hollowing out of the soil skeleton, composed of coarse particles. The reclosure of the pore subsequent to the collapse of the skeleton resulted in a sudden increase in pore water pressure. The value of P1-3 continued to increase at 294 min of rainfall (Fig. 10b) . This is because the fine particles that migrated to the slope toe obstructed a portion of the pores, thereby inhibiting the seepage channel and making rainwater drainage difficult. Consequently, the pore water pressure continued to increase. The value of P2-3 in the E2 test exhibited a gradual increase at 276 min of rainfall, reaching a peak at 303 minutes (Fig. 10c). This was subsequently followed by a sharp decline. This may be due to the fact that granite residual soil in the area exhibit negative dilatancy (Chen et al. 2024). When shear damage occurring on the slope, the pores within the soil became smaller in size, thereby the pore water pressure in the soil continued to increase. The pore water pressure was dissipated after the landslide occurred. The E3 test exhibited a greater number of bends in each pore water pressure curve, with the sensor value initially increasing and subsequently decreasing. It indicates that multiple localized cracks appeared in the slope during the period of the E3 test, which is consistent with the experimentally observed phenomenon. It is also noteworthy that the response time of the peak pore water pressure in the soil in the vicinity of the sliding surface are all smaller than the response time of the peak water content. This suggests that there is a hysteresis in the response of the pore water pressure. This is in accordance with the fact that the majority of landslides occur subsequent to the peak rainfall intensity (Dai et al. 1999a).

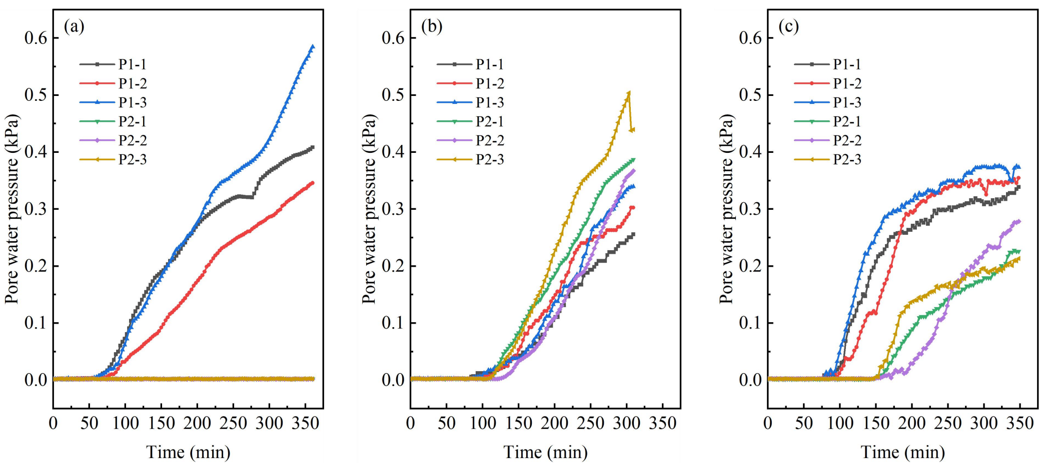

Figure 10. Pore water pressure-time curves. **(a)** E1 slope. **(b)** E2 slope. **(c)** E3 slope.

5 Discussion

The essence of rainfall-induced landslides is the occurrence of a series of complex interactions between rainwater infiltrated into the slope and the geotechnical body (Xu 2007; Hou et al. 2017). Therefore, an in-depth analysis of rainfall infiltration affect can aid in understanding the cause of landslides. In this study, rainfall infiltration is affected by the thickness of the residual layer, which makes the failure pattern of the granite weathered crust slope significantly different from that of related studies in the granite area (Wu et al., 2022; Yin et al., 2023). When the residual layer is thin, rainfall infiltration results in the rapid saturation of the residual layer and the occurrence of seepage. The fine particles in the soil continue to accumulate towards the slope toe under seepage, which impedes the drainage of the slope toe. This leads to a continuous rise in pore water pressure. Concurrently, the incease in the fine particle content of the soil enhances the likelihood of soil liquefaction (Monkul and Yamamuro 2011; Monkul et al. 2016). The slope toe is destabilized first. The loss of fine particles destroys the soil structure, which in turn leads to the disintegration of the soil. The soil

https://doi.org/10.5194/egusphere-2024-2138
Preprint. Discussion started: 8 January 2025

undergoes large-scale flow under water flow (Fig. 11a). When the residual layer thickens, in-slope seepage is primarily observed at the soil-rock interface under rainfall infiltration. The seepage is not strong, and there is less loss of fine particles from the soil. The integrity of soil body is relatively good. The continuous accumulation of water towards the slope toe results in the soil saturation, which in turn causes the formation of cracks at the slope toe. Besides, the soil-rock interface forms a region of high pore water pressure, which has low shear strength. The soil body tends to slide along the soil-rock interface direction under the traction and drag of seepage. The landslide finally occurred as traction failure at the slope toe (Fig. 11b). As the residual layer becomes thicker, the in-slope seepage is no longer apparent. Rainfall infiltration results in the formation of cracks in the middle and top of slope where stress concentrations occur. The cracks are subsequently filled with water, generating hydrostatic pressure. The cracks inside the slope are constantly expanding and penetrating. The slope experienced thrust-type damage under the combined action of hydrostatic pressure and gravity. The sliding surface exhibits a circular arc shape as a result of the shearing failure in cohesive materials(Fig. 11c).

In addition, there is a question worth discussing. This study was conducted based on model tests, and the model materials utilized were collected in the field and are considered to be remodeled samples. It should be noted that the constructed slope model may differ somewhat from the actual situation, which may result in limited practical usability of the results of this research. Consequently, this study investigated the correspondence between the actual residual layer thickness and landslides, as well as to analyze the consistency between the findings and the model test results. Figure 12 depicts landslide 11, which is compared to the failure pattern of E1 slope. The landslide almost involves the entire mountain, lacking an obvious sliding surface. Its movement was similar to that of a debris flow. The E1 experiment result did not exhibit a severe flow-slip phenomenon comparable to Landslide 11 due to the limitations of the test conditions. Figure 13 depicts landslide 15, which is compared to the failure pattern of E2 slope. The landslide has obvious sliding surface and is located at the boundary between the residual and completely weathered layers. The trailing edge of the landslide displays a pronounced scarp with a semicircular planar profile, accompanied by evidence of traction damage. The field investigation also found that Landslide 15 was responsible for the triggering of several secondary landslides on the mountain. Figure 14 depicts landslide 8, which is compared to the failure pattern of E3 slope. The trailing edge and sidewalls of the landslide exhibit numerous tensile cracks, which correspond with the emergence of multiple cracks on the slope at the conclusion of the E3 experiment. The leading edge of the mountain appeared to uplift phenomenon, with a height of about 20 cm. Secondary cracks were found on the road. The landslide exhibits feature of thrust type. The test results in this study showed that the slopes were susceptible to damage at shallow depths under short-term heavy rainfall. This finding is consistent with the results of the field investigation.

Finally, the model tests conducted in this study were subject to the following limitations. Firstly, the selection of the thickness of the residual layer of the slope model was primarily based on the assumption that the thickness of the residual layer exerts an influence on the slope damage pattern. Consequently, the residual layer thickness was not taken into account sufficiently finely. Secondly, the rainfall design of the test was based on actual rainfall scenarios and did not consider the impact of different rainfall characteristics on slope damage pattern, such as the influence of rainfall intensity and rainfall duration. In the next phase of research, tests should be designed to study slope failure pattern under the combined effect of residual layer thickness and rainfall characteristics. This will facilitate the wider application of the research findings.

https://doi.org/10.5194/egusphere-2024-2138
Preprint. Discussion started: 8 January 2025

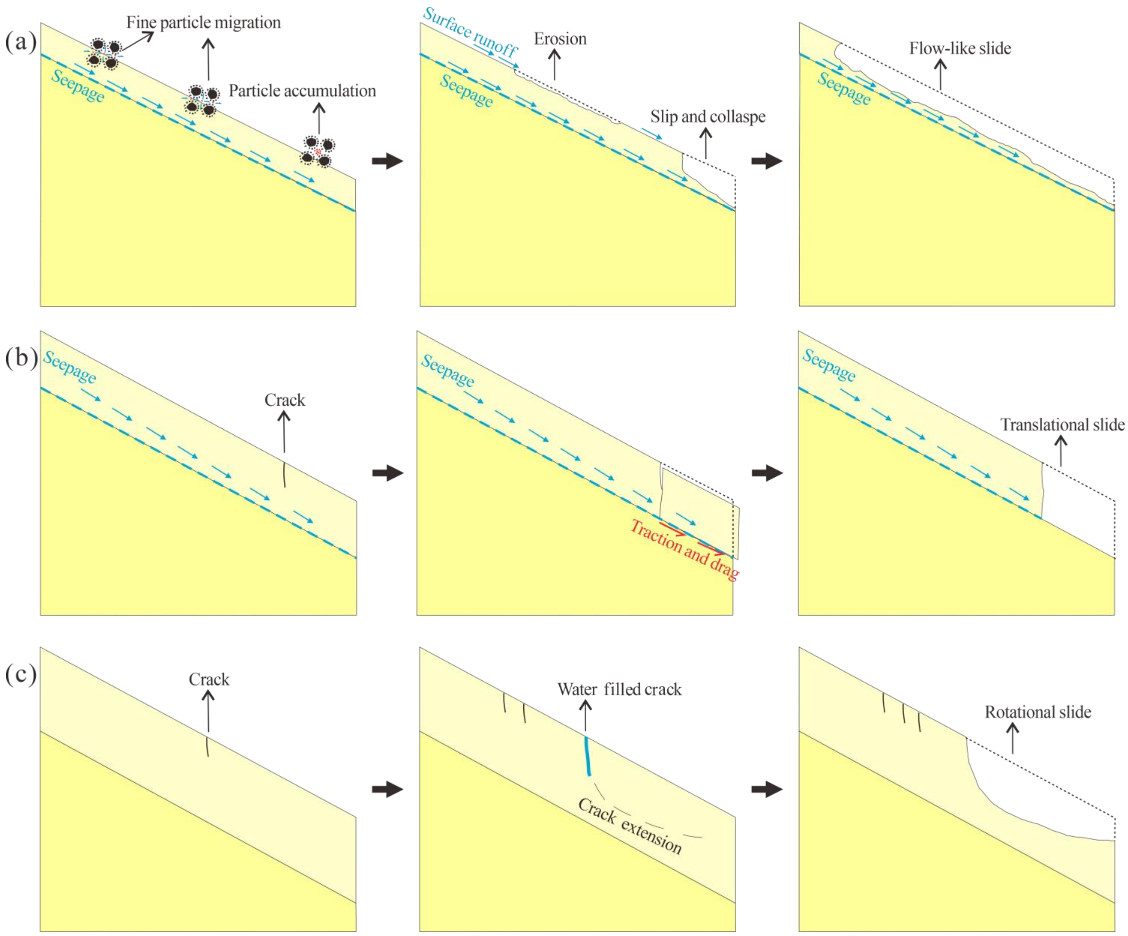

Figure 11. The process of destruction of slopes. **(a)** E1 slope. **(b)** E2 slope. **(c)** E3 slope.

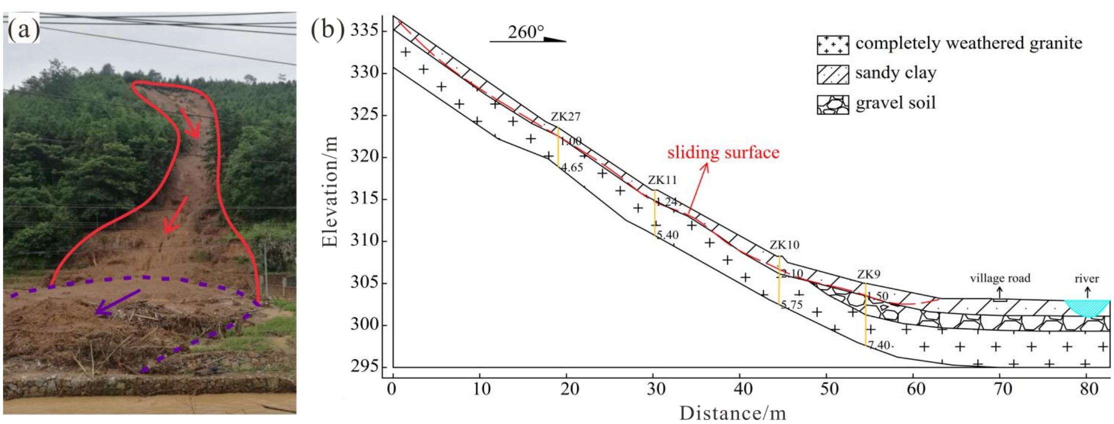

Figure 12. No.11 landslide. **(a)** landslide panoramic view. **(b)** landslide sectional view.

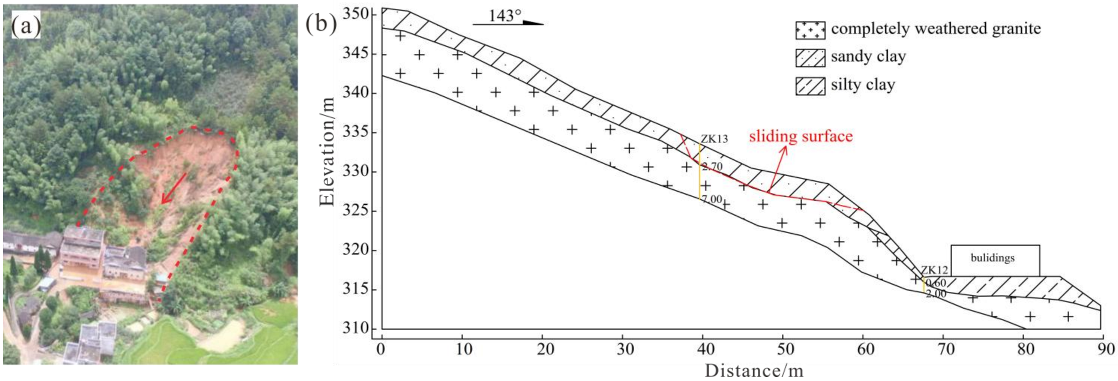

Figure 13. No.15 landslide. **(a)** landslide panoramic view. **(b)** landslide sectional view.

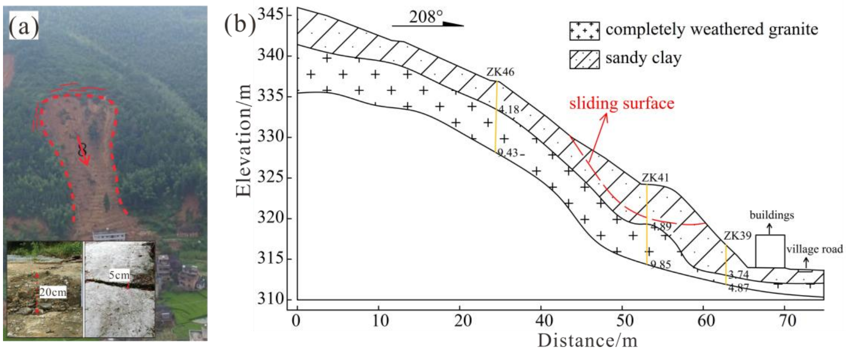

Figure 14. No.8 landslide. **(a)** landslide panoramic view. **(b)** landslide sectional view.

6 Conclusion

In this study, the hydrological response and damage mechanism of slopes with different granite weathered crusts were investigated by physical model test against the background of group-occurring landslides in Mibei Village, Longchuan County, Guangdong Province, China. The main conclusions are as follows.

Rainfall that infiltrates the soil-rock interface may stagnate due to the difference in permeability coefficients between the residual and weathered layer. Residual soil near the soil-rock interface becomes saturated more rapidly and is prone to seepage along the interface. The thinner the residual layer, the shorter the time for rainfall infiltration to reach the soil-rock interface, and the more pronounced the phenomenon of water stagnation and seepage at the interface, which in turn affects the mode and mechanism of slope failure. No evidence of strong seepage is observed within the slope when the residual layer thickness was 30 cm. In the event of the short term and high-density rainfall, the slope with a residual layer of 10 cm is susceptible to overall flow-slip damage without an apparent sliding surface; the slope with a residual layer of 20 cm is prone to traction sliding at the slope toe with sudden, where the sliding surface is at the soil-rock interface; the E3 slope with a residual layer of 30 cm tends to a thrust-type slide at the middle of the slope, where the sliding surface with a circular arc shape is within the residual layer and the damage process is gradual. The landslides are all shallow damage.

Data availability. The data used to support the findings of this study are available from the corresponding author upon request.

Author contributions. CJ carried out the artificial model tests, analyzed the experimental data and wrote the manuscript. WJ and YS participated in the tests and analyzed part of the data. GQ guided the design and implementation of the tests, as well as revised the content of the manuscript.

Competing interests. The authors declare no competing interests.

References

https://doi.org/10.5194/egusphere-2024-2138
Preprint. Discussion started: 8 January 2025

An, R., Kong, L. W., Li, C. S., and Luo, X. Q.: Strength attenuation and microstructure damage of granite residual soils under hot and rainy weather, Chin. J. Rock Mech. Eng., 39(9):1902–1911, https://doi.org/10.13722/j.cnki.jrme.2020.0073, 2020.

Bai, H. L., Feng, W. K., Yi, X. Y., Fang, H. Y., Wu, Y. Y., Deng, P. C., Dai, H. C., and Hu, R.: Group-occuring landslides and debris flows caused by the continuous heavy rainfall in June 2019 in Mibei Village, Longchuan County, Guangdong Province, China, Nat. Hazards, 108(3), 3181–3201, https://doi.org/10.1007/s11069-021-04819-1, 2021.

Bai, H. L., Feng, W. K., Li, S. Q.,Ye, L. Z., Wu, Z. T., Hu, R., Dai, H. C., Hu, Y. P., Yi, X. Y., and Deng, P. C.: Flow-slide characteristics and failure mechanism of shallow landslides in granite residual soil under heavy rainfall, J. Mt. Sci., 19(6),1541–1557, https://doi.org/10.1007/s11629-022-7315-8, 2022.

Branco, L. P., Gomes, T. A,. Cardoso, A. S., and Pereira, C. S.: Natural variability of shear strength in a granite residual soil from porto, Geotech Geol Eng., https://doi.org/10.1007/s10706-014-9768-1, 2014.

Chen, X. P., Zhou, Q. J., and Cai, X. Y.: Physical properties and shear strength characteristics of high liquid limit granite residual soil, Chin. J. Geotech. Eng., 33(6), 901–908, 2011.

Coutinho, R. Q., Silva, M. M., Santos, A. N, and Lacerda, W. A.: Geotechnical characterization and failure mechanism of landslide in granite residual soil, J. Geotech. Geoenviron., 145(8), 1–16, https://doi.org/10.1061/(ASCE)GT.1943-5606.0002052, 2019.

Cui, P., Guo, C. X., Zhou, J. W., Hao, M. H., and Xu, F. G.: The mechanisms behind shallow failures in slopes comprised of landslide deposits, Eng. Geol., 180, 34–44, http://doi.org/10.1016/j.enggeo.2014.04.009, 2014.

Chen, J. Y., Gong, Q. H., Wang, J., and Yuan, S. X.: Damage cause and mechanism of well-vegetated soil slopes under extreme rainfall: a case study, Front. Earth Sci., 12, https://doi.org/10.3389/feart.2024.1402798, 2024.

Dai, F. C., Lee, C. F., and Wang, S. J.: Analysis of rainstorm-induced slide-debris flows on natural terrain of Lantau Island, Hong Kong. Eng. Geol., 51(4), 279–290, https://doi.org/10.1016/s0013-7952(98)00047-7, 1999a.

Feng, W. K., Bai, H L., Lan, B., Wu, Y. Y., Wu, Z. T., Yan, L. Z., and Ma, X. J.: Spatial–temporal distribution and failure mechanism of group-occurring landslides in Mibei Village, Longchuan County, Guangdong, China, Landslides, 19, 1957–1970, https://doi.org/10.1007/s10346-022-01904-9, 2022.

Harianto, R., Satyanaga, N. A., Leong, E. C., and Song, N. Y.: Effects of groundwater table position and soil properties on stability of slope during rainfall, J. Geotech. Geoenviron., 136(11), 1555–1564, https://doi.org/10.1061/(ASCE)GT.1943-5606.0000385, 2010.

Herrada, M. A., Gutierréz-Martin, A., and Montanero, J. M.: Modeling infiltration rates in a saturated/unsaturated soil under the free draining condition, J. Hydrol., 515, 10–15, https://doi.org/10.1016/j.jhydrol.2014.04.026, 2014.

Hou, X. K., Sai, K., and Li, T. L.: Water infiltration characteristics in loess associated with irrigation activities and its influence on the slope stability in Heifangtai loess highland, China, Eng. Geol., 234(1), 198–209, http://doi.org/10.1016/j.enggeo.2017.12.020, 2018.

Iverson, R. M.: Landslide triggering by rain infiltration, Water Resour. Res., 36(7), 1897–1910, https://doi.org/10.1029/2000wr900090, 2000.

Jia, B. Z., Wu, Y. Y., Feng, W. K., Bai, H. L., Xue, Z. H., and Zhao, J. C.: $1^{\#}$ debris flow disaster characteristics and movement process in Mibei Village, Longchuan County, Sci. Tech. Eng., 24(9), 3576–3585, https://doi.org/10.12404/j.issn.1671-1815.2304262, 2024.

Li, C. S., Kong, L. W., Shu, R. J., An, R., and Zhang, X. W.: Disintegration characteristics in granite residual soil and their relationship with the collapsing gully in South China, Open Geosci., 12(1), 1116–1126, https://doi.org/10.1515/geo-2020-0178, 2020.

Liu, X. Y., Zhang, X. W., Kong, X. M., and Wang, G.: Effect of cementation on the small-strain stiffness of granite residual soil, Soils Found., 61(2), 520–532, https://doi.org/10.1016/j.sandf.2021.02.001, 2021.

Li, Y., Xue, K. X., Zhao, Y., Wang, L. L., Bi, J., Wang, T. Y., Wang, S. F., and Zhang, B.: Study on the stability and disaster mechanism of layered soil slopes under heavy rain, Bull. Eng. Geol. Env., 82, 272, https://doi.org/10.1007/s10064-023-03277-2, 2023.

Lu, X. B., Ye, T. L., Cui, P., Hu, K. H., and Chen, X. Q.: Numerical investigation on the initiation mechanism of debris-flow under rainfall, J. Mt. Sci., 8(4), 619–628, https://doi.org/10.1007/s11629-011-2129-0, 2011.

Monkul, M. M., and Yamamuro, J. A.: Influence of silt size and content on liquefaction behavior of sands, Can. Geotech. J., 48(6), 931–942, https://doi.org/10.1139/t11-001, 2011.

Monkul, M.M., Etminan, E., and Senol, A.: Influence of coefficient ofuniformity and base sandgradation on static liquefaction of loose sands with silt, Soil Dyn. Earthq. Eng., 89, 185–197, https://doi.org/10.1016/j.soildyn.2016.08.001, 2016.

Marin, R. J., and Velai, M. F.: Influence of hydraulic properties on physically modelling slope stability and the definition of rainfall thresholds for shallow landslides, Geomorphology, 351(15), 106976, https://doi.org/10.1016/j.geomorph.2019.106976, 2020.

Nian, G. Q., Chen, Z. H., Zhu, T. Y., Zhang, L. F., and Zhou, Z. H.: Experimental study on the failure of fractured rock

https://doi.org/10.5194/egusphere-2024-2138
Preprint. Discussion started: 8 January 2025

slopes with anti-dip and strong weathering characteristics under rainfall conditions, Landslides, 21, 165–182, https://doi.org/10.1007/s10346-023-02142-3, 2024.

Qi, X., Li, Q. H., Jiao, Y. Y., and Tan, F.: Vertical zoning criteria and engineering geological characteristics of super-thick layer granite weathering crust in Wuzhou City, J. Eng. Geol., 30(2), 407–416, https://doi.org/10.13544 /j.cnki.jeg.2020-159, 2022.

Rahardjo, H., Lee, T. T., Leong, E. C., and Rezaur, R. B.: Response of a residual soil slope to rainfall, Can. Geotech. J., 42(2), 340–351, https://doi.org/10.1139/t04-101, 2005.

Su, S. X., and Zhang, Y. X.: Similarity criterion in physical simulation of rainfall and sheet flow, Transactions of the CSAE, 28(11), 93–98, https://doi.org/10.3969/j.issn.1002-6819.2012.11.016, 2012.

Tang, G. P., Huang, J. S. , Sheng, D. C., and Sloan, S. W.: Stability analysis of unsaturated soil slope under random rainfall patterns, Eng. Geol., 45(1), 322–332, https://doi.org/10.1016/j.enggeo.2018.09.013, 2018.

Wang, Q., Tang, D. X., Zhang, Q. Y., and Zhao, J. Z.: A study on the structure and composition on granite residual soil in the eastern China, J. Jilin Univ. (Earth Sci.), 21(1), 73–81, 1991.

Wakatsuki, T., and Matsukura, Y.: Lithological effects in soil formation and soil slips on weathering-limited slopes underlain by granitic bedrocks in Japan, Catena, 72(1), 153–168, http://doi.org/10.1016/j.catena.2007.05.002, 2008.

Wang, D. Y., Zeng, J., Wang, J., and Zhou, M.: Effect of dry-wet cycle on stability of granite residual soil slope, IOP Conference Series: Earth Env. Sci., 526, 12046, https://doi.org/10.1088/1755-1315/526/1/012046, 2020.

Wu, S. B., Zhao, R. H., Liao, L. P., Yang, Y. C., Wei, Y., and Wei, W. Z.: Failure mode of rainfall-induced landslide of granite residual soil, southeastern Guangxi Province, China, Earth Surf. Dynam., 10, 1079–1096, https://doi.org/10.5194/esurf-10-1079-2022, 2022.

Wang, J., Gong, Q. H., Yuan, S. X., and Chen, J.: Combining soil macropore flow with formation mechanism to the development of shallow landslide warning threshold in South China, Front. Earth Sci., 10, 1048427, https://doi.org/10.3389/feart.2022.1048427, 2023.

Xia, J. W., Cai, C. F., Wei, Y. J., and Wu, X. L.: Granite residual soil properties in collapsing gullies of south China: spatial variations and effects on collapsing gully erosion, Catena, 174, 469–477, https://doi.org/10.1016/j.catena.2018.11.015, 2019.

Xu, Z. M.: Vegetation and macropores in vadose zones of hill slopes, Earth Sci. Front., 14(6), 134–142, 2007.

Xu, X. T., Jian, W. B., Wu, N. S., and Xu, X.: Model test of rainfall-induced residual soil slope failure, China J. Highw. Transp., 31(2), 270–279, https://doi.org/10.19721/j.cnki.1001-7372.2018.02.029, 2018.

Xu, X. T., Jian, W. B., Wu, N. S., Xu, X., and Liu, J. L.: Unsaturated seepage characteristics of slope under rainfall infiltration, Earth Sci., 433(3), 922–932, http://doi.org/10.3799/dqkx.2017.580, 2018.

Yin, L., Huang, C. S., Hao, S. R., Miao, L., Li, J. Y., Qiu, Y. G., and Liu, H.: Experimental study on the stability of shallow landslides in residual soil, Water, 15(21), 3732, https://doi.org/10.3390/w15213732, 2023.

Zhang, Y. B., Zhang, Y., Chen, G., and Yin, M. Y.: The system of engineering category dividing of granite residual soil, Acta Geo. Sin., 18(2), 89–93, 1997.

Zhang, Y. Y.: Eroding soil types and their management counter measures of granite regions in Guangdong Province, China, J. Mt. Sci., 27(1), 49–53, https://doi.org/10.16089/j.cnki.1008-2786.2009.01.003, 2009.

Zhang, S., Zhang, X. C., Pei, X. J., Wang, S. Y., Huang, R. Q., Xu, Q., and Wang, Z. L.: Model test study on the hydrological mechanisms and early warning thresholds for loess fill slope failure induced by rainfall, Eng. Geol., 258, 105135, https://doi.org/10.1016/j.enggeo.2019.05.012, 2019.

Zhang, C. Y., Zhang, M., Zhang, T. L., Dai, Z. W., and Wang, L. Q.: Influence of intrusive granite dyke on rainfall-induced soil slope failure, Bull. Eng. Geol. Env., 79(10), 5259–5276, https://doi.org/10.1007/s10064-020-01895-8, 2020.

Zhang, B. C., Ning, Y. B., Tang, H. M., Ding, B. D., Fang, K., and Zou, Z. X.: Study on the evolutionary process of interbedded anti-inclined slope block-flexure toppling in the upper Yalong River, Bull. Eng. Geol. Env., 82, 240, https://doi.org/10.1007/s10064-023-03223-2, 2023.

Zeng, L., Bian, H. B., Shi, Z. N., and He, Z. M.: Forming condition of transient saturated zone and its distribution in residual slope under rainfall conditions, J. Cen. South Univ., 24(8), 1866–1880, https://doi.org/10.1007/s11771-017-3594-6, 2017.

Zhu, X. H.: Analysis of geological hazard characteristics and influencing factors in Longchuan County, Guangdong Province, West Resour., 21(2), 106–108, https://doi.org/10.16631/j.cnki.cn15-1331/p.2021.02.038, 2021.

Zhen, J., Yang, X. J., Wang, B. Z., Fan, H. H., and Meng, M. Q.: Study on the destruction of backfilled loess slopes by short-term extreme rainfall erosion, Bull. Eng. Geol. Env., 82, 406, https://doi.org/10.1007/s10064-023-03426-7, 2023.